Foundering Lithosphere Imaged Beneath the Southern Sierra Nevada, California, USA

Oliver S. Boyd,* Craig H. Jones, Anne F. Sheehan

Seismic tomography reveals garnet-rich crust and mantle lithosphere descending into the upper mantle beneath the southeastern Sierra Nevada. The descending lithosphere consists of two layers: an iron-rich eclogite above a magnesium-rich garnet peridotite. These results place descending eclogite above and east of high *P* wave speed material previously imaged beneath the southern Great Valley, suggesting a previously unsuspected coherence in the lithospheric removal process.

The Sierra Nevada mountain range of California is one of the highest (about 3 km mean elevation) in the United States; however, the crust is only 35 km thick (*1*) and requires some unusual structure in the mantle. Xenoliths (*2*) and volcanic rocks (*3*, *4*) suggest that the upper mantle source for these materials, beneath the Sierra Nevada, changed from an eclogite facies garnet pyroxenite to a garnet-free spinel peridotite about 4 million years ago (Ma). Eclogitic rocks may still be present in the upper mantle below the Sierra Nevada (*5*), and knowing where and how much is left constrains how lithospheric material is removed and how continental crust grows and changes beneath mountain ranges (*6*). To determine whether there are any eclogitic rocks left, we used three-dimensional models of *P* and *S* wave speeds to define compositional and thermal characteristics of the lithosphere. We measured attenuation to correct the velocities for anelastic effects, which include temperature and hydration. The corrected wave speeds are subsequently termed anharmonic wave speeds and compared with laboratory predictions.

Low Pn velocities directly beneath the high Sierra (*7*, *8*) and high attenuation in the upper mantle in the region (*9*) are consistent with high temperature, low-density material. Shear wave splitting measurements determined from the seismic phase SKS (*10*, *11*) (Fig. 1) indicate strong seismic anisotropy oriented N80°E beneath the central Sierra, probably because of the presence of strained, olivine-rich, peridotitic mantle. Less splitting beneath the eastern and western Sierra may indicate largely isotropic material, such as eclogite (*12*), little strain, or a vertical fast axis of anisotropy. The region of large SKS splitting and low Pn velocity correlates well with high mantle electrical conductivity that is probably due to 1% partial melt beneath the southern Sierra Nevada (*13*). These observations are consistent with the presence of a peridotitic uppermost mantle near asthenospheric temperatures near the Sierran crest today.

We recorded 40 teleseismic events that yielded 800 seismic wave traces on 24 broadband seismometers (Fig. 1). We measured direct *P* wave and S_{fast} and S_{slow} wave travel time delays (t_P, t_{S_f}, and t_{S_s}) and S_{fast} and S_{slow} wave path–integrated attenuation, Δt^* (*14*), to invert for variations in *P* wave speed, v_P, fast and slow *S* wave speeds (v_{S_f} and v_{S_s}), and fast- and slow-oriented *S* wave attenuation ($Q_{S_f}^{-1}$ and $Q_{S_s}^{-1}$). These were combined to examine variations in the ratio of *P* wave to *S* wave velocity, v_P/v_S, and transverse *S* wave anisotropy. Our tomographic inversions reduce the variance of the data by more than half of that available, whereas measurement noise and station and event statics account for the remainder (*15*).

The tomographic models reveal regions of alternating high and low velocity and attenuation that dip ~55° to the east southeast (Fig. 2). The region of high *P* wave velocity at 36.4°N extends from –119.5°W to –118°W and may be what has been referred to as the Isabella anomaly. The volume above this anomaly consists of a slow *P* and *S* wave region. The *S* wave velocities decrease more across this contrast than do the *P* wave velocities, giving rise to an increase in the v_P/v_S ratio. These seismic anomalies trend northeast (Fig. 3C).

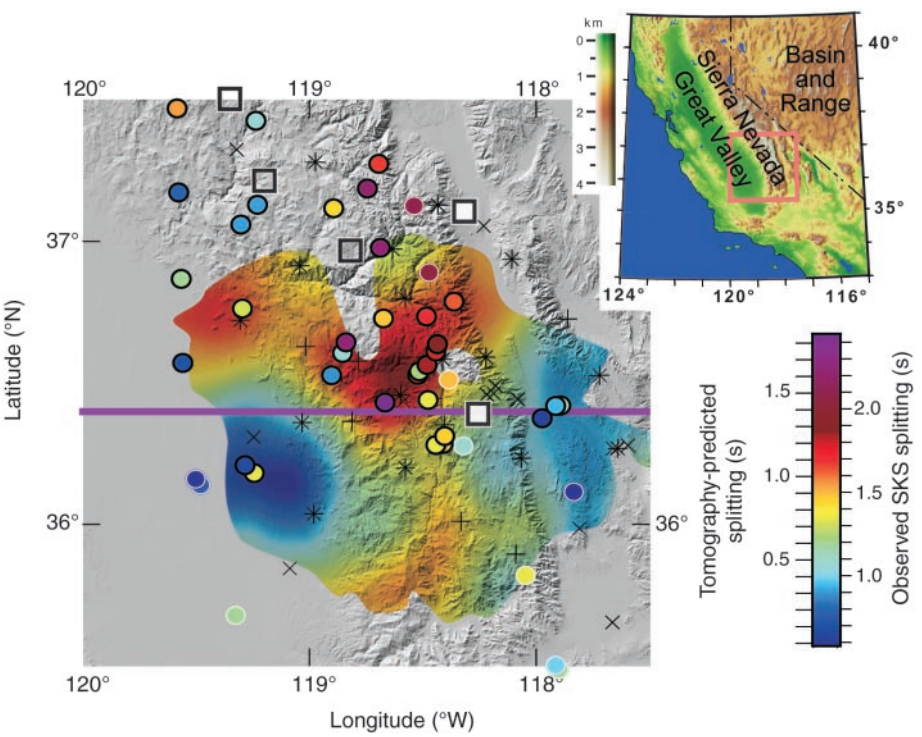

Fig. 1. Topographic map of the southern Sierra Nevada overlain with tomographically predicted shear wave splitting (this study) and independently determined SKS splitting measurements, filled circles with white (*10*) or black (*11*) outline. Map of Nevada and California with pink outline of study area given in the upper right for reference. The SKS measurements are placed at 125-km depth along the SKS ray path. The tomographically predicted splitting time is determined by integrating differences between the fast and slow *S* wave speed models in the upper 200 km for regions with greater than 150-km thickness of resolution greater than 0.5. Thick purple line crossing at 36.4°N is the latitudinal position of the vertical slices in Fig. 2. The plus symbols are seismograph stations used for the tomography, the multiplication symbols are stations used to measure SKS splitting, and the asterisks, plus symbols overlain by multiplication symbols, are stations used for both tomography and SKS splitting. The open boxes are garnet peridotite and garnet pyroxenite xenolith localities; solid boxes are spinel peridotite xenolith localities.

Department of Geological Sciences, University of Colorado at Boulder, 2200 Colorado Avenue, Boulder, CO 80309–0399, USA.

*To whom correspondence should be addressed. E-mail: oliver.boyd@colorado.edu

Upon vertically integrating the differences in S_{fast} and S_{slow} travel times for the top 200 km, we are able explain more than 50% of the variance of the SKS splitting measurements (Fig. 1 and fig. S1) (*15*), an independent verification of our subsurface distribution in anisotropy. The SKS measurements were not used in the inversion; we used only the orientation of fast *S* wave speed derived from the splitting analysis. The shallow depth for the origin of the splitting (<200 km) is consistent with the 1-s variation in splitting amplitudes over short distances (<50 km) and inconsistent with splitting distributed over greater depths.

Attenuation is needed to distinguish between the effects on wave speed from thermal and compositional variations (*16*, *17*). Anisotropy (*12*) and Poisson's ratio (*18*) can then be used to constrain the composition (Table 1). Because of anelasticity, temperature variations will cause seismic velocities and attenuation to vary predictably (*19*). We interpret deviations from the thermal relationship as being caused by variations in composition.

Because the dipping layer of low wave speeds is accompanied by low attenuation, temperatures are relatively low (~200 K lower than the material to the east), and partial melt or partially water-saturated minerals are not likely present. This leaves some sort of compositional effect producing, in addition to low velocities, a high v_P/v_S ratio and variable anisotropy. High v_P/v_S ratios can indicate an increase in the amount of pyroxene and garnet relative to olivine or a decrease in the Mg number [Mg/(Mg + Fe)]. The variable anisotropy is more difficult to interpret. Lower anisotropies can be from an absence of olivine, an absence of strain, or a heterogeneously strained peridotite. In response to infilling asthenosphere, the low anisotropy in the inferred region of spinel peridotite (Fig. 2D) could be anisotropic but have a near-vertical axis of orientation. Normally isotropic lithologies like eclogites might be anisotropic if pervasively cut by dikes or if the pyroxenes have become preferentially aligned (*15*). The large anisotropy appearing below the dipping layer of high *P* wave velocities may reflect lateral extrusion of asthenospheric peridotite in response to delaminating mantle lithosphere.

Ambiguity in interpreting the tomographic results can be reduced by examining the xenoliths erupted nearby in the central Sierra Nevada. There are three groups of xenoliths: garnet pyroxenites and garnet peridotites (both erupted before 8 Ma) constituting the old mantle lithosphere (*2*, *20*) and fertile, olivine-rich, garnet-free spinel peridotites (erupted since 4 Ma) with an asthenospheric affinity (*2*). Chemically, the garnet and pyroxene in the pyroxenites tend to have low Mg, whereas the olivine in the peridotites has a higher Mg number (*2*). This observation means that the garnet pyroxenite will have higher v_P/v_S ratios relative to the peridotites.

We calculated the *P* and *S* wave speeds (*15*, *21*) for a range of expected compositions and compare these values to our observations of anharmonic wave speed (*15*) to broadly determine the mineralogy and Mg numbers in the observed seismic anomalies (Fig. 3). The modal proportions for the garnet pyroxenite xenolith samples are predicted to be about 65% clinopyroxene and 35% garnet (*22*). The Mg number ranges from 0.6 to 0.9 for the clinopyroxenes and 0.3 to 0.6 for the garnet (*2*). The composition that best matches our seismic observations averages 70% pyroxene and 30% garnet (*15*). Compositions having as much as 40% garnet would be acceptable if a Reuss average, as opposed to the Voight-Reuss-Hill average (*23*) used here, is favored. One garnet peridotite sample has 75% olivine, 15% orthopyroxene, 5% clinopyroxene, and 5% garnet (*24*), whereas the Mg numbers are reported to be on average 0.91, 0.91, 0.92, and 0.85 for those minerals, respectively (*2*). Our seismically determined composition averages 75% olivine, 20% pyroxene, and 5% garnet. The young peridotite samples are devoid of garnet and average 80% olivine, with the remainder orthopyroxene, clinopyroxene, and spinel (*25*). Their Mg numbers average 0.89, 0.89, 0.87, and 0.67, respectively (*2*). Because a majority of the young samples have been classified as harzburgites, we restrict our analysis to clinopyroxene-free assemblages. We find this composition has on average 80% olivine, 16% pyroxene, and 4% garnet (*26*).

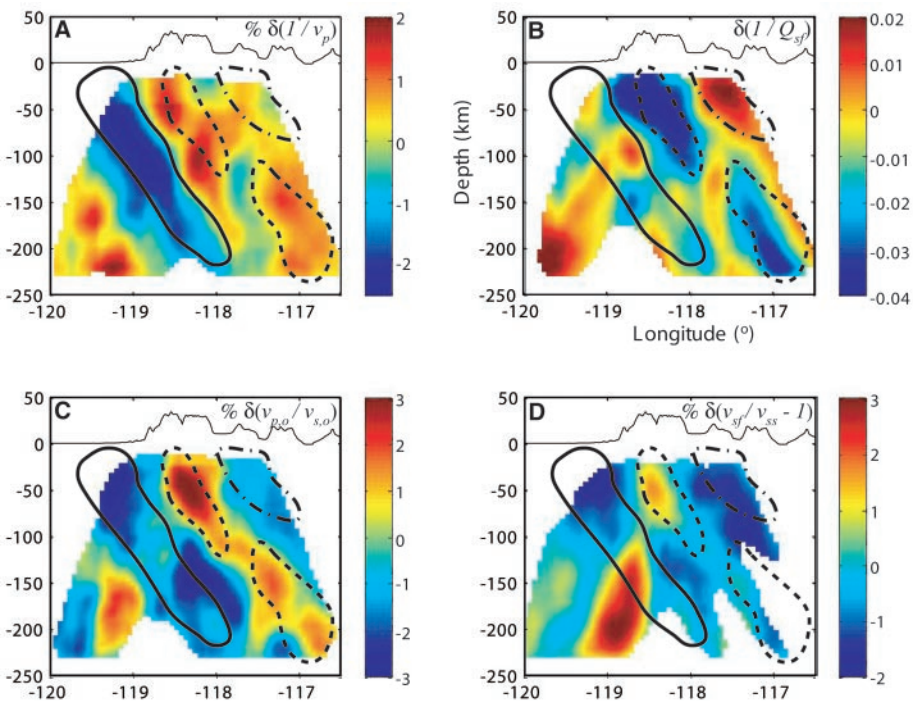

Fig. 2. Vertical slices of our tomographic models and derived quantities:percent change in *P* wave slowness (**A**), change in attenuation (**B**), percent change in anharmonic v_P/v_S ratio where v_S is taken from the average of the fast and slow models (**C**), and shear wave anisotropy where the slow model is derived as residuals from the fast model (**D**). The solid lines indicate regions of descending garnet peridotite, and the dashed lines delineate regions of garnet pyroxenite. The regions of low velocities and high attenuation above the garnet pyroxenite are presumably the infilling of asthenospheric spinel peridotite (dashed-dot outlines). Topography is depicted with 10 times vertical exaggeration.

Table 1. Changes observed in geophysical properties in the mantle from different causes. The asterisk indicates that the attenuation will only increase if high temperatures are required to produce melt (*15*). The question mark indicates that anisotropy may increase or change orientation if melt pockets and/or bands are favorably oriented.

Increasing factor	v_P	v_P/v_S	Attenuation	Anisotropy	Density
Temperature	Decrease	Increase	Increase	No change	Decrease
Melt	Decrease	Increase	*	?	Decrease
Magnesium	Increase	Decrease	No change	No change	Decrease
Garnet/olivine ratio	Increase	Increase	No change	Decrease	Increase

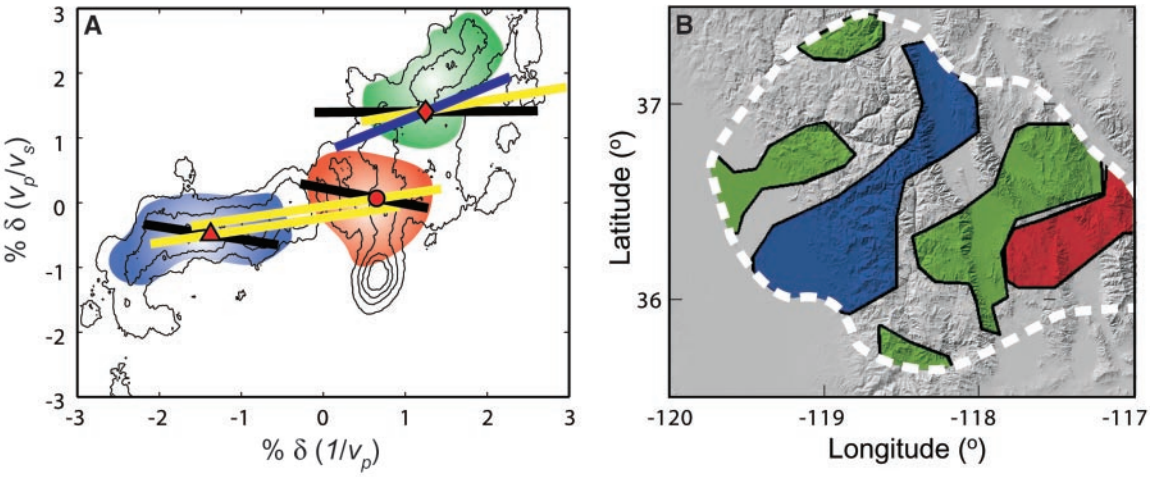

Fig. 3. (**A**) Percent change in anharmonic v_P/v_S ratio versus percent change in anharmonic *P* wave slowness for a range of model compositions at a pressure of 3 GPa and a range of temperatures. Compositions defined in the text that best match the seismic observations are garnet pyroxenite (red diamond) at 1200°C, spinel peridotite (red circle) at 2000°C, and garnet peridotite (red triangle) at 1000°C. Thick black lines represent ranges in composition where garnet is substituted for pyroxene. For the garnet pyroxenite, garnet varies from 20% (right end of black line, slower wave speeds) to 40%; the spinel peridotite, 0 to 10%; and the garnet peridotite, 0 to 10%. Yellow lines represent a 400 K variation in temperature (900 to 1300°C), with faster wave speeds (to the left) accompanying lower temperatures. The blue line spans the range of Mg numbers for the garnet pyroxenite samples. Contours denote anharmonic *P* wave slowness and v_P/v_S from our Sierran tomography from 75- to 100-km depth. Each contour interval represents 20% of the data. Colored areas correspond to compositional regions outlined in the tomography of Fig. 2 and shaded areas in the 100-km-depth slice (**B**). Garnet pyroxenite, green; spinel peridotite, red; and garnet peridotite, blue. Compositional zones in (B) derived from tomography using composition relations (*15*) with *P* wave slowness, Poisson's ratio, anisotropy, and attenuation. The white dashed line delimits the part of the tomography model with resolution greater than 0.4.

Many eclogites are seismically fast because they have a large proportion of garnet and much of the pyroxene is in the form of jadeite (*27*). The xenoliths found here, however, have large amounts of clinopyroxene (*24*) and very little jadeite (*2*). The garnet pyroxenites are therefore slower than common eclogites and have a higher v_P/v_S ratio relative to the peridotites (Fig. 3A). A comparison of the characteristics of the seismic anomalies to calculated values for mineral assemblages (Fig. 3A) reveals that the dipping layer of high velocity is the garnet peridotite; the low velocity layer above, garnet pyroxenite; and the seismically intermediate region above and to the east, asthenospheric spinel peridotite (Fig. 2). A map view of the older garnet-bearing assemblages at 100-km depth indicates a northeast strike to this structure (Fig. 3B). The seismically determined compositions imply that, at 100-km depth, densities increase from close to neutrally buoyant garnet peridotite below to very dense, negatively buoyant ($\Delta\rho \approx 185$ kg/m^3) garnet pyroxenite above.

Although we have suggested specific differences in composition and temperature for the three rock assemblages identified, the most robust conclusion is that three distinct rock types exist in the upper mantle beneath the Sierra Nevada. This observation is made possible by correcting measured *P* and *S* wave seismic velocities for attenuation and comparing these values to laboratory results. The apparent dip of the two garnet-bearing packages and the asymmetry of the package (garnet peridotite to the west of the garnet pyroxenite) are important constraints on the mechanism of removal of this material. The asymmetry resembles delamination of stratified mantle lithosphere from the crust and is inconsistent with most numerical models of removal by development of a Rayleigh-Taylor instability (*28*), although such asymmetry might be produced by an initially asymmetric instability (*29*). The eastward plunge of this body indicates that either material has moved directly downward or somewhat to the east relative to the overlying crust, in contrast to motion to the west relative to the crust inferred from older images of this structure (*5*). Imaging one of the very few (if not the only) examples of ongoing removal of mantle lithosphere from beneath continental crust, this tomography provides some of the best observational constraints on the process of removing dense material from continental crust.

References and Notes

1. B. Wernicke *et al*., *Science* **271**, 190 (1996).
2. M. Ducea, J. Saleeby, *J. Geophys. Res.* **101**, 8229 (1996).
3. C. R. Manley, A. F. Glazner, G. L. Farmer, *Geology* **28**, 811 (2000).
4. G. L. Farmer, A. F. Glazner, C. R. Manley, *Geol. Soc. Am. Bull.* **114**, 754 (2002).
5. G. Zandt, *Int. Geol. Rev.* **45**, 213 (2003).
6. M. Ducea, *J. Geophys. Res.* **107**, 10.1029/2001JB000643 (2002).
7. C. H. Jones, H. Kanamori, S. W. Roecker, *J. Geophys. Res.* **99**, 4567 (1994).
8. M. M. Fliedner *et al*., *Geology* **24**, 367 (1996).
9. H. H. Al-Khatib, B. J. Mitchell, *J. Geophys. Res.* **96**, 18129 (1991).
10. J. Polet, H. Kanamori, *Geophys. J. Int.* **149**, 313 (2002).
11. C. H. Jones, R. A. Phinney, *Geol. Soc. Am. Abstr. Prog.* **31** (no. 7), A-481 (1999).
12. N. I. Christensen, W. D. Mooney, *J. Geophys. Res.* **100**, 9761 (1995).
13. M. Ducea, S. K. Park, *Geophys. Res. Lett.* **27**, 2405 (2000).
14. A. F. Sheehan, S. C. Solomon, *J. Geophys. Res.* **97**, 15339 (1992).
15. Please refer to the supporting online material on *Science* Online for more information about seismic methods, resolution, and calculation of mineral properties.
16. O. S. Boyd, A. F. Sheehan, in *Lithospheric Structure and Evolution of the Rocky Mountain Region*, K. E. Karlstrom, G. R. Keller, Eds. (*Geophys. Monogr. Am. Geophys. Union*), in press.
17. S. Karato, *Geophys. Res. Lett.* **20**, 1623 (1993).
18. N. I. Christensen, *J. Geophys. Res.* **101**, 3139 (1996).
19. I. Jackson, *Annu. Rev. Earth Planet. Sci.* **21**, 375 (1993).
20. F. C. W. Dodge, J. P. Lockwood, L. C. Calk, *Geol. Soc. Am. Bull.* **100**, 938 (1988).
21. B. R. Hacker, G. A. Abers, *Geochem. Geophys. Geosys.* **5**, 10.1029/2003GC000614 (2004).
22. J. Saleeby, M. Ducea, D. Clemens-Knott, *Tectonics* **22**, 10.1029/2002TC001374 (2003).
23. J. P. Watt, G. F. Davies, J. O'Connell, *Rev. Geophys. Space Phys.* **14**, 541 (1976).
24. M. Ducea, J. Saleeby, *Contrib. Mineral. Petrol.* **133**, 169 (1998).
25. H. G. Wilshire *et al*., *U.S. Geol. Surv. Prof. Pap. 1443* (1988), p. 179.
26. Garnet is used for the spinel peridotite composition because we are considering seismic velocities at 3 GPa, by which pressure spinel would have transformed to garnet.
27. R. G. Coleman, D. E. Lee, J. B. Beatty, W. W. Brannock, *Geol. Soc. Am. Bull.* **76**, 483 (1965).
28. G. A. Houseman, P. Molnar, *Geophys. J. Int.* **128**, 125 (1997).
29. M. Jull, P. B. Kelemen, *J. Geophys. Res.* **106**, 6423 (2001).

30. Thanks to P. Molnar and L. Farmer for helpful discussion and B. Phinney and several land use agencies (U.S. Forest Service, Sequoia and Kings Canyon National Parks, and Bureau of Land Management) for help in obtaining the data. We also acknowledge two anonymous reviewers and L. Rowan for thorough reviews. This work was supported by NSF grants 9526974 and 0003747 and a Cooperative Institute for Research in Environmental Research Sciences fellowship.

Supporting Online Material

www.sciencemag.org/cgi/content/full/305/5684/660/DC1
Materials and Methods
Figs. S1 to S3
Tables S1 and S2

15 April 2004; accepted 24 June 2004